A Simulation Study on the Transport Phenomena in Ultrafiltration

Licínio M. Ferreira[1], *Paulo Brito and António Portugal*
Department of Chemical Engineering, University of Coimbra, Pólo II, Pinhal de Marrocos, 3030 Coimbra, Portugal

Maarten Blox and Piet Kerkhof
Laboratory of Separation Technology and Transport Phenomena, Faculty of Chemical Engineering and Chemistry, Eindhoven University of Techonology, P.O.Box 513, 5600 MB Eindhoven, Netherlands

Abstract

A coupled model of concentration polarization and membrane transport is used to study the crossflow ultrafiltration of PEG-3400 solutions. For the intramembrane transport, the model incorporates the binary friction model (BFM) derived by Kerkhof [4] and that is a modification of the Maxwell-Stefan-Lightfoot equation. Good agreement between model predictions and experimental data (apparent rejections and pressure drops as function of the flux) has been obtained. A value of 0.49 for the equilibrium partition coefficient K, the only adjustable parameter, was found. The model predictions also enabled us to study the effects of circulation velocity and partition coefficient on the apparent rejection and to get an insight into the concentration profiles in the polarization layer and in the membrane.

Keywords: Apparent rejection; Adaptive method; Maxwell-Stefan; Transport; Ultrafiltration.

Introduction

Modeling of mass transport phenomena present in the separation of solutes using inert membranes is important for the design and/or optimization of these new separation processes. In recent years, there has been an increased awareness on these type of processes since they can be an alternative to the conventional separations processes like distillation, centrifugation and others. They also find applications in a variety of fields, being the most prominent the food and bioprocess areas.

A number of mathematical models and algorithms for their solution have been explored for the description of the transport of components through membranes. Some of them are special cases of the generalized Maxwell-Stefan equations [1-2] and can be derived from either statistical-mechanics or thermodynamics of irreversible processes [3]. In fact, the approach based on the Maxwell-Stefan theory for the transport in both the polarization layer and the membrane give a rigorous description of the problem and the thermodynamics effects involving more than one species can be well predicted. However, this kind of mathematical formulation results, for the binary case, in two partial differential equations (PDE's) defined in two different spatial regions, corresponding to the boundary layer and the membrane and the use of commercial packages such the PDECOL and PDASAC to achieve a transient solution is difficult, since they were developed to solve straightforward PDE's. In most of the studies the steady-state behavior is considered, where the problem is described by a set of ODE's and the solution is obtained by employing numerical methods based on finite differences. With this approach the coupled equations are solved via an iterative procedure and in many situations, problems of convergence and stability of the numerical method occur.

This work focuses on the ultrafiltration of PEG solutions. For the intramembrane transport the binary friction model derived by Kerkhof [4 -5] was used. That is a modification of the Maxwell-Stefan-Lightfoot equation, and includes both interspecies (diffusive) and species-wall forces. The numerical scheme used for solution of the equations is based on the application of an adaptive method with grid refinement developed by Brito and Portugal [6].

[1] Author to whom the correspondence should be addressed

Mathematical Model

The modeling of the transport of solutes through membranes involves a couple solution of two transport models. The first model describes the transport phenomena in the concentration polarization layer on the feed side adjacent to the membrane, while the second model deals with the intramembrane (inside membrane pores) transport.

The governing equations for the unsteady-state transport of species through the membrane can be described by the continuity equations. For the polarization layer (see Figure 1), we have,

$$\frac{\partial (c)}{\partial t} = -\frac{\partial (N)}{\partial z} \tag{1}$$

where the flux per unit area of the membrane is written as $(N) = -([D] + [D_t])\frac{\partial c}{\partial t} + u_v c$, in which the Fickian molecular and turbulent diffusion matrixes are given by $[D] = [B]^{-1}[\Gamma_c]$ and $[D_t] = D_t [I]$, respectively; for the membrane, the equations are written as

$$\varepsilon \frac{\partial (c')}{\partial t} = -\frac{1}{\tau}\frac{\partial (N_m)}{\partial z} \tag{2}$$

where N_m is the flux per square meter of membrane area.

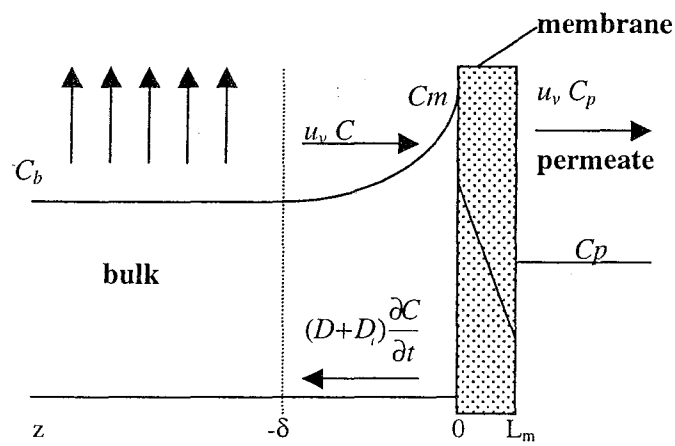

The intramembrane transport can be subdivided into intermolecular fricction between different components, and the effective friction of each component with the wall. The detailed momentum balance for each component, and the averaging over the pore cross section, results in the binary friction model (BFM) that is an extension of the Lighfoot model [3],

$$\frac{x_i}{RT}\nabla_{T,P}\mu_i + \frac{c_i \bar{V}_i}{c_t R T}\nabla P = \sum_{j=1}^{n}\frac{x_i N_j - x_j N_i}{c_t D_{ij}} - \frac{1}{B_o}k_i \phi_i u_i \tag{3}$$

where the last term of right side of the eq. (3) enables us to quantify the friction between the components and the membrane. This term includes the fractional viscosity coefficients k_i that can be evaluated from the bulk mixture viscosity data.

Finally, considering the binary case that involves the transport of a single solute, we obtain for the boundary layer,

$$\frac{\partial c}{\partial t} = -\frac{\partial N}{\partial z} \tag{4}$$

with $N = -(D + D_t)\frac{\partial c}{\partial t} + u_v c$ and $D = D_{12}\Gamma_c$.

For the intramembrane transport, we have,

$$\varepsilon \frac{\partial c'}{\partial t} = -\frac{1}{\tau}\frac{\partial N_m}{\partial z} \tag{5}$$

From eq. (3), by converting the chemical potential gradients in concentration gradients and developing the equation in terms of molar fluxes, N_m is given by,

$$N_m = -\frac{\Gamma_c}{G}\frac{\partial c'}{\partial z} + u_v \frac{F}{G} c', \quad \text{where } F = \left(\frac{1}{D_{12}} + \frac{c_t^2 \bar{V}_1 \bar{V}_2}{B_0} k_2\right)\frac{\tau}{\varepsilon} \text{ and}$$

$$G = \left(\frac{1}{D_{12}} + \frac{c_t}{B_0}(\phi_2 k_1 \bar{V}_1 + \phi_1 k_2 \bar{V}_2)\right)\frac{\tau}{\varepsilon},$$

with boundary conditions,

$z = -\delta_{pol}$: $c = c_b$

$z = 0$ (interface polarization layer/membrane): $c' = K c$ and $N = N_m$

$z = L_m$(interface membrane/permeate): $N = u_v c_p$ ($c_p = c'/K$)

and initial conditions,

$t = 0$: $c = c_b$ for $z = -\delta_{pol}$ and $c = c' = 0$ for $z > -\delta_{pol}$.

For turbulent conditions the diffusion mechanism in the polarization layer should incorporate an additional transport contribution by the turbulent eddies. The usual procedure for prediction of D_t is to proceed through the calculation of kinematics viscosity, υ_t. Defining the turbulent Schmidt number as $Sc = \upsilon_t / D_t$ and considering that for most practical design purposes Sc value is taken equal to 1, i.e., $D_t = \upsilon_t$. If the turbulent viscosity is taken to vary according to Vieth correlation,

$$\frac{\upsilon_t}{\upsilon} = \left(\frac{2}{9}\Pi\sqrt{3}\right)^3 \left(\frac{f}{2}\right)^{3/2} \left(y^+\right)^3 \tag{6}$$

The reduced distance from the membrane wall is expressed as $y^+ = \dfrac{y < u_t > \sqrt{f/2}}{\upsilon}$ in which the fanning friction factor, is evaluated using the Blasius equation, $f = (0.3164/4)\, Re^{-0.25}$. According to Kerkhof [4], a region limited by $y^+ \leq 5$ was considered as having the sufficient distance for the development of the composition profiles within of the boundary layer of thickness δ.

The coupled model of concentration polarization and membrane transport presented provides a consistent procedure for predicting the concentration and molar flux profiles throughout the system, the permeate concentration c_p and the apparent rejection of the solute, given by,

$$R_{app} = 1 - \frac{c_p}{c_b} \tag{7}$$

For the total pressure gradient over the membrane $\Delta P_{tot} = \Delta P_{flow} + \sigma \Delta \prod$, in which $\Delta \prod$ is the osmotic pressure difference that depend on the concentrations on both membrane sides and of the osmotic reflection coefficient σ, the following expression was used for ΔP_{flow} evaluation,

$$\Delta P_{flow} = \frac{\tau R T}{\varepsilon B_o} \int_0^{Lm} c_t \sum_{i=1}^{2} k_i N_i \bar{V}_i dz \tag{8}$$

The relationship between the pressure differences ΔP and the flux Uv for experiments with pure water enables the determination of the membrane resistance R_m.

$$R_m = \frac{\Delta P}{\eta_w J_v} \qquad (9)$$

where $R_m = \frac{L_m \tau}{B_o \varepsilon} = \frac{8 L_m \tau}{r_p^2 \varepsilon}$. Hence, the ratio ε/τ can be evaluated from the R_m value and the geometrical properties of the membrane.

Numerical Procedure

The adaptive mesh algorithm was developed for one-dimensional evolutive systems of Algebraic-Differential Equations that can be resumed by the following general model:

$$F(\underline{u}_t, \underline{u}, \underline{u}_z, \underline{u}_{zz}) = 0$$
$$G(\underline{u}) = 0$$

subjected to the boundary conditions: $\underline{u}(z^L, t) = \underline{u}^L(t)$ and $\underline{u}(z^R, t) = \underline{u}^R(t)$ and the initial condition: $\underline{u}(z,0) = \underline{u}^0(z); \quad z \in \left[z^L, z^R\right]$. The algorithm can be structured in two main stages: estimation of the discretization error and identification of the adaptive sub-domains; and solution of the sub-problems generated in the first stage, by the introduction of an adaptive grid technique.

Stage I - Discretization

The error estimation is based on the comparison of the solution obtained by solving the original problem on two different grids: a fine and a coarse grid (Grids of level 2 and 1, respectively). Initially, the fine grid is constructed by the bissection of each interval of the coarse one. The nodes in level 1 grid, that do not satisfy the error criterion, are grouped together with the level 2 nodes placed between them, to define the sub-domains over which the adaptive sub-problems are generated and then solved.

Stage II - Adaptive Integration of the Sub-problem

The sub-problems are generated with increasing refinement level, by the repetition of the procedure described in Stage I, until every node in every grid verifies the tolerance condition associated with the error estimated by:

$$EU^i_{j,k+1} = Wh^i_{j,k+1} - W2h^i_{j,k+1}; \quad j = 1, \cdots, NP_{n-1}, \quad i = 1, \cdots, NPDE$$

In this case, $EU^i_{j,k+1}$ represents the approximation to the spatial error, in a node j of a grid of refinement level n; $Wh^i_{j,k+1}$ and $W2h^i_{j,k+1}$ are the approximations to the component i of the solution, obtained through integration between the times t_k and t_{k+1}, on the finer (level n) and the coarser (level n-1) grids, respectively; NP_{n-1} is the number of nodes in the grid of level n-1; and $NPDE$ is the number of partial differential equations of the problem.
The sub-domains of level n+1 are obtained by joining all nodes n-1 that satisfy the condition:

$$\left|EU^i_{j,k+1}\right| > TOL_i; \quad i = 1, \cdots, NPDE$$

In each refinement procedure, the profiles of the solution are computed by interpolation of the profiles of level 2, at all the intermediary positions.
The algorithm is coupled with a strategy for the treatment of boundary conditions in the refinement sub-problems that simply defines fixed Dirichlet conditions on each internal bound. The position of each bound, for the refinement level n+1 (for n = 2, ... , N_{MAX-1}, where N_{MAX} is the maximum refinement level) are coincident with the positions of the first nodes of level n-1 that verify the

specified tolerance. The constant value of the boundary conditions is given by the solution obtained in the integration over the level n-1 grid. This kind of procedure is very simple and prevents discontinuities on the overall profiles but tends to introduce significant errors in the solution, in very specific cases.

The model is divided in the overall length in relation to the concentration (normalized by the bulk conditions). The fluxes are later calculated using the concentration profiles. The spatial coordinate ($-\delta \leq z \leq L_m$) is also normalized using the overall length: $z^* = \frac{z+\delta}{L_m+\delta}$. Therefore, in the bulk position: $z = -\delta$, $z^* = 0$, and for the permeate position: $z = L_m$, $z^* = 1$. The differential equations that describe the time evolution of the concentrations are spatially discretized by finite differences approximations (either on the polarization layer as on the membrane sides) and solved simultaneously. Initially we assume a zero concentration profile on the whole domain (with the obvious exception of the bulk border). The bulk border is treated as a fixed *Dirichlet* condition with $C = C_b$. The inner border (which represents the transition between the polarization layer and the membrane) and the permeate border are treated with the introduction of two nodes (very close to one another) that represent the inner and outer conditions related to the membrane. For the inner border (positioned at $z = 0$; $z_{ib}^* = \frac{\delta}{L_m+\delta}$) the solution on both nodes is calculated by the solution of two algebraic equations: the equality of the fluxes on both positions and the equilibrium condition. The strategy used for the treatment of the permeate border (positioned at $z = L_m$; $z^* = 1$) is similar and it is based on the solution of two algebraic equation also: the equality of fluxes, which has to satisfy the border condition: $N = u^v \times C_p$; and the equilibrium condition.

Results and discussion

Comparison of model predictions with experimental data

In order to validate the model, we used data from ultrafiltration experiments of PEG-3400 performed by Box, [7] in a cross-flow ultrafiltration module containing a tubular polysulfone membrane of 1 meter length, with two separated permeate sections. Samples for analysis were obtained from the second section of the tube, where the entrance effects are absent. The operating conditions of the system under study are given in Table 1.

Regarding the physical properties of the solution, we used $\eta_{sp} = 0.1(\eta_{int})\rho_p + 0.0033(\eta_{int}\rho_p)^2$ and $\eta_{int} = 6.04\times10^{-5}M_n^{0.90}$ with M_n(number-averaged molecular Mass) = 3158, for the calculation of the PEG3400 viscosity. From the viscosity data, the fractional viscosity coefficients k_1 e k_2 were estimated according to the following relationships: $k_1 = k_2(1+\eta_{sp}/\phi_1)$, where k_2 may be related directly to the pure solvent (water), η_w=ct RT k_2. For the determination of the molecular Fickian diffusion coefficient in aqueous PEG-3400 solutions, the following relation was taken into account: $D = (5\omega_p + 1.37)\cdot10^{-10}$ m^2.s^{-1}.

Table 1-Conditions used in the simulation of ultrafiltration of PEG3-400 solutions

Membrane characteristics	Solution properties	Flow conditions
L_m=5.10^{-7} m	c_b=2.78·10^{-3} kmol/m^3	u_t = 1.08; 1.57 m/s
R_m=1.62·10^{16}. Uv+5.39x10^{12}m^{-1}	M=3600	δ =86.10^{-6} m
r_p=9.00.10^{-9} m^2	$\bar{V}_1$ =2.83 m^3/kmol	
MWCO=50 kDa	$\bar{V}_2$ =0.018 m^3/kmol	
ε = 0.50	η_w =8.0·10^{-4} Pa.s	
	T= 298 K	

The comparison of experimental apparent rejections of PEG-3400 with the values predicted by the model are presented in Fig. 1. As can be seen, the model is able to describe well the experimental results for K = 0.49. In Fig.2, it is also visible a good agreement between the pressure drop calculated for σ= 0 and the ones measured.

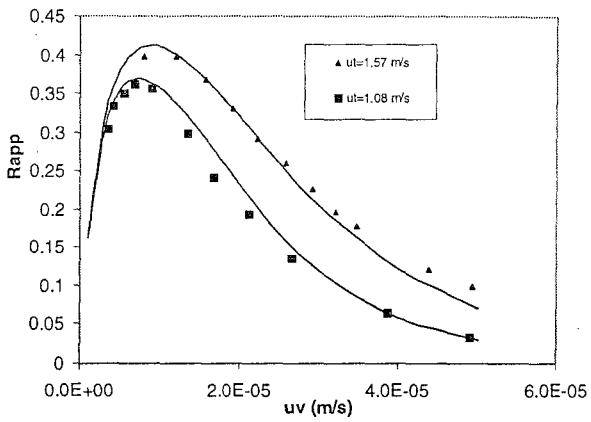

Figure 1 – Apparent rejection of PEG-3400 as function of the flux at two different circulation velocities. The predictions are the solid lines whereas the experimental data are presented by the symbols.

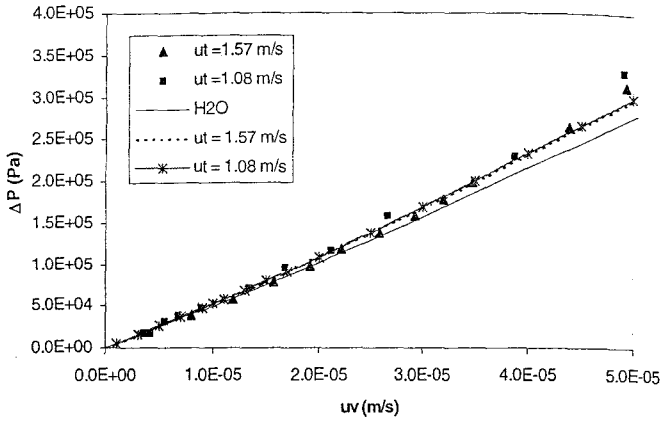

Figure 2 – Pressure drop vs membrane flux. The predictions are the solid lines whereas the experimental data are presented by the symbols.

Effect of circulation velocity u_t

The apparent rejection is affected by the circulation velocity along membrane tube as shows the Fig. 1. It can be observed that increasing u_t results in a increase of the apparent rejection. Since the turbulent contribution for the mass transport in the polarization layer increases at high circulation velocities, the amount of solute accumulated on the surface membrane is expected to decrease. This will correspond to a lower value of the membrane surface concentration and thus less solute will be transported through the membrane and hence, the rejection will increase.

Effect of equilibrium partition coefficient K

Concentrations in the membrane pore are related to the interfacial bulk concentrations through the partition coefficients. Once the interfacial region is very small and therefore the differences in the chemical potential are negligible, to assume interfacial equilibrium conditions ($K_i = c_i'/c_i$) is a valid approximation. The K_i value is determined by geometrical factors and by specific interactions of solute and pore wall. For spherical solutes in cylindrical pores and according to the exclusion theory, K_i only depends on the ratio of the molecular radius and the pore radius: $K_i = (1 - \lambda_i)^2$. Thus, for a given solute, the decrease of the partition coefficient is consistent with the use of membranes that exhibit lower pore radius and thereby, the solute concentration in the pores will tend to increase. Consequently, high values of solute rejection will be obtained as is depicted in Fig. 3.

Concentration Profiles

For a flux of 10^{-5} m/s and at circulation velocity of 1.04 m/s, the evolution of PEG-3400 concentration along the spatial coordinate for various time values are shown in Figures 4a and 4b. The conditions used in this simulation corresponds to the ultrafiltration experiment of PEG-3400 reported by Kerkhof [4]. In Fig. 4a, the behavior of the solute transport in the polarization layer can be observed together with the propagation of the bulk concentration towards the membrane driven by the

contribution of the convective and diffusive fluxes. At higher times the concentration near the membrane increases surface due to the exclusion of the solute by the membrane, therefore originating a back diffusion is generated influencing strongly the evolution of concentration inside the membrane. This phenomena is illustrated in Fig. 4b.

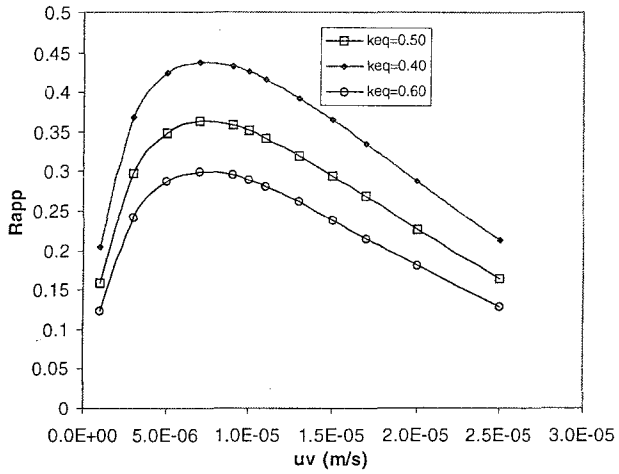

Figure 3 – Effect of equilibrium partition coefficient on the apparent rejection of PEG-3400

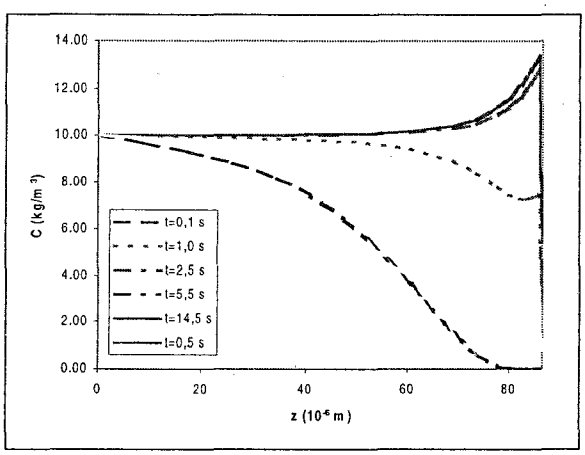

Figure 4a – Concentration profiles of PEG-3400 as a function of time in the polarization layer.

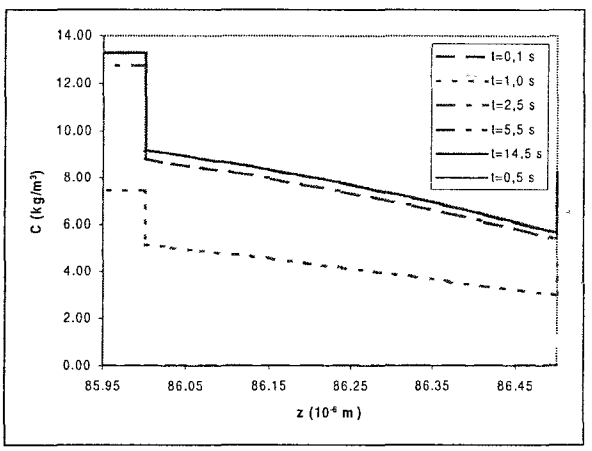

Figure 4b – Concentration profiles of PEG –3400 as function of time in the membrane.

Conclusions

A coupled model of concentration polarization and membrane transport described by the binary friction model (BFM) is used to study the crossflow ultrafiltration of PEG-3400 solutions.

A numerical procedure based on the adaptive method with grid refinement, in which the model differential equations are spatially discretized by finite differences and solved simultaneously, was able to give the solution of the system without much computational power and yield a rigorous solution of the problem. It has been shown that the solution predicts quite well the apparent rejection of PEG-3400 and the pressure drop as a function of the flux. The model is capable of predicting the influence of fundamental physico-chemical parameters and operating conditions on the apparent rejection of the solute. In fact, the influence of some of these parameters namely, the circulation velocity and the equilibrium partition coefficient was shown in this study. The predictions of the model also provides a good insight regarding the concentration and flux profiles in the polarization layer and in the membrane.

The numerical description of the ultrafiltration model used is versatile and allows in the future to extend this study to the multicomponent transport.

Nomenclature

c: molar concentration ($kmol.m^{-3}$)
B_0: permeability parameter (m^2)
D: Fick diffusion coefficient ($m^2 .s^{-1}$)
D_{12}: Maxwell-Stefan diffusion coeficient ($m^2 .s^{-1}$)
D_t: turbulent diffusion coefficient ($m^2 .s^{-1}$)
k: fractional viscosity coefficient
K: equilibrium partition coefficient
L_m: membrane thickness (m)
M: molecular mass ($kg .kmol^{-1}$)
N: flux with respect to stationary coordinate ($kmol.m^{-2}.s^{-1}$)
P: pressure (Pa)
r_p: pore radius (m)
R: gas constant ($J.kmol^{-1}.K^{-1}$)
x: mole fraction
t: time (s)
T: temperature (K)
u_t: circulation velocity ($m.s^{-1}$)
u_v: average permeate flux ($m.s^{-1}$)
$\bar{V}$: specific molar volume ($m^3.kmol^{-1}$)
z: spatial coordinate (m)
( ): vector
[ ]: square matrix

Greek letters

δ: thickness of polarization layer (m)
ε:porosity
ϕ: volume fraction
Γ_c: thermodynamic factor
τ: tortuosity
η:viscosity (Pa.s)
μ: chemical potential ($J.kmol^{-1}$)
ρ: mass concentration ($kg.m^{-3}$)
ω_p: weight fraction (kg.kg-1)

Subscripts

b: bulk
m: membrane
p: permeate
pol: polarization
t: total
w: water.

References

[1] T.R. Noordman and J.A. Wesselingh, *J. of Membrane Science* 210 (2002) 227-243

[2] W.M. Deen, *AIChE Journal* (1987) 1409-1425

[3] E.N.Lightfoot, *Transport in Living Systems*, Wiley, New York, 1974

[4] P.J.A.M. Kerkhof, *The Chem. Eng. Journal* 64 (1996) 319-343

[5] P.J.A.M. Kerkhof, M. M. Geboers and K. Ptasinski, *The Chem. Eng. Journal* 83 (2001) 107-121

[6] P.M.P. Brito and A.A.T.G.Portugal, *Adv. Comput. Meth. In Eng.,* ACOMEN'98, in Proceeding of Conference on Advanced Computational Methods in Engineering

[7] M.J.J. Blox, *MSc. Thesis,* Eindhoven University of Technology (June 2003)